Time-Domain Testing Strategies and Fault Diagnosis for Analog Systems

HONG DAI AND T. MICHAEL SOUDERS, MEMBER, IEEE

Abstract—**An efficient approach is presented for functional testing and parameter estimation of analog circuits in the time domain. The test equations are based on the sensitivity matrix, which can be obtained simultaneously with the nominal solution vector. An example is given, with results based on actual measurement data. Practical considerations, including the effects of ambiguity groups, measurement errors, and time skew are covered. The approach can be directly extended to nonlinear circuits.**

I. Introduction

THE OBJECTIVE of this paper is to present an efficient approach for functional testing and fault diagnosis of analog circuits. To accommodate nonlinear elements more conveniently, the focus is on analysis and testing performed in the time domain. Several authors have discussed the diagnosability of dynamical circuits theoretically [1]–[3]. In this work we address several practical issues related to calibration, functional testing, alignment, and fault diagnosis:

1) efficient parameter estimation, necessary for trimming and alignment, and fault identification;
2) accurate response predictions for arbitrary input signals, important for calibration and functional testing;
3) test point selection (test nodes and input signal levels and waveforms), important in achieving adequate test coverage with minimum cost.

The approach extends that presented in [4], [5] to include time-domain analysis, and can be directly extended to include nonlinear systems. Two stages of computation, pretest and post-test, are required. In the pretest stage, the following tasks are performed: modeling the circuit under test, simulating the time-domain response to one or more specific input signals, creating a sensitivity matrix, and performing test point selection and a testability analysis on the sensitivity matrix.

During testing, reference time-domain input signals are applied to the circuit under test using signal levels selected in the pretest stage. A waveform recorder is used to record the input response(s) at the previously selected test nodes.

In the post-test stage, the time-domain measurement data are used together with the sensitivity matrix to estimate the actual network parameters. Accurate predictions of the circuit's response to other arbitrary inputs can be made by performing response simulations using the updated parameter estimates. If the actual circuit parameters are substantially different from the nominal values on which the sensitivity matrix is based, then iteration involving recalculating or updating the sensitivity matrix will also be required in this stage.

Manuscript received April 26, 1989; revised September 8, 1989.

H. Dai was with the Department of Electrical Engineering, Ohio University, Athens, OH. She is now with the Department of Electrical Engineering, Lafayette College, Easton, PA 18042.

T. M. Souders is with the National Institute of Standards and Technology, Gaithersburg, MD 20899.

IEEE Log Number 8931822.

II. General Approach

The general approach we have taken is to formulate the test equations in the linear form

$$S\frac{\Delta p}{p} = \Delta v \qquad (1)$$

where S is the sensitivity matrix corresponding to a given time-domain input signal, with

$$s_{nj} = \frac{\partial v_n}{\partial p_j} p_j.$$

p_j is the nominal value of the jth parameter, $\Delta p/p$ is the normalized vector of deviations of the parameter values from nominal, Δv is the vector of measured deviations (from nominal) of the output, and n is a discrete time index. If there are m measurement nodes, then there will be m equations of the form given by (1).

The true parameter values can be determined from time-domain measurements of the output, by solving (1) for $\Delta p/p$. When the number of discrete time points is greater than the number of parameters, as is usually the case, (1) can be solved using a least squares approach. On the other hand, for greater efficiency, the number of measurements can be reduced to the number of parameters, and an exact solution can be obtained. In [5], a process for selecting a nearly optimal subset of measurement points is presented, based on a QR factorization of S.

A. Time-Domain Sensitivity Matrix

For simplicity, we use a linear network to illustrate the procedure for obtaining the time-domain sensitivity matrix. The procedure can be generalized to handle nonlin-

ear networks. In the time domain, the system equations of a linear network can be written as [6]

$$C\dot{v} + Gv = w \tag{2}$$

where v is the voltage and current vector, $\dot{v}$ represents dv/dt, G is the resistive element matrix, C is the reactive element matrix, and w is the input vector.

The time interval $(0, T)$ is divided into $N + 1$ discrete points $(0, t_1, t_2, \cdots, T_N)$, where $t_N = T$. At each time point, the solution of (2) is determined first, then the sensitivity of the output with respect to all parameters, $\partial v/\partial p$, can be obtained simultaneously with the solution vector.

The initial condition v_0 can be obtained by the dc solution of the system. At an arbitrary time point t_n, (2) becomes

$$C\dot{v}_n + Gv_n = w_n. \tag{3}$$

To solve (3), we use the difference equations:

$$\dot{v}_n = (1/h)(v_n - v_{n-1}), \qquad \text{for } n = 1 \tag{4.a}$$

$$\dot{v}_n = (2/h)(v_n - v_{n-1}) - \dot{v}_{n-1}, \qquad \text{for } n \geq 2 \tag{4.b}$$

where

$$h = t_n - t_{n-1}. \tag{5}$$

To get higher accuracy and efficiency, differentiation formulas with variable step size and order could be applied to (3).

Substituting (4.a) and (4.b) into (3), respectively, we get

$$[(1/h)C + G]v_n = (1/h)Cv_{n-1} + w_n, \qquad \text{for } n = 1 \tag{6.a}$$

$$[(2/h)C + G]v_n = [(2/h)C - G]v_{n-1} + (w_{n-1} + w_n), \qquad \text{for } n \geq 2. \tag{6.b}$$

Once the matrices G and C are known from the nodal formulation, (6.a) and (6.b) are applied directly.

In order to find sensitivities $\partial v/\partial p$, we differentiate both sides of (3) with respect to p:

$$C\frac{\partial \dot{v}_n}{\partial p} + G\frac{\partial v_n}{\partial p} + \frac{\partial C}{\partial p}\dot{v}_n + \frac{\partial G}{\partial p}v_n = 0. \tag{7}$$

Let us denote

$$s_n = \frac{\partial v_n}{\partial p} \text{ and } u_n = -\left(\frac{\partial C}{\partial p}\dot{v}_n + \frac{\partial G}{\partial p}v_n\right). \tag{8}$$

Substituting (8) into (7), we have

$$C\dot{s}_n + Gs_n = u_n. \tag{9}$$

By again applying the discrete-difference equations to (9), we obtain the following, from which the sensitivity vectors, s_n, can be calculated:

$$[(1/h)C + G]s_n = (1/h)Cs_{n-1} + u_n, \qquad \text{for } n = 1 \tag{10.a}$$

$$[(2/h)C + G]s_n = [(2/h)C - G]s_{n-1} + (u_{n-1} + u_n), \qquad \text{for } n \geq 2. \tag{10.b}$$

Note that the coefficient matrices of (6) and (10) are the same. As a result, the factorized coefficient matrices from the solution of (6) can be stored and used again to calculate sensitivities s_n in (10).

B. Iteration

To improve the accuracy of parameter estimation when the linear model of (1) is inadequate, i.e., when the true values deviate substantially from their nominal values, an iterative process is implemented.

1) Solve the linear system $S^k \Delta p^k/p^k = \Delta v^k$ to obtain $\Delta p^k/p^k$, where k stands for the kth iteration.
2) Update the sensitivity matrix to S_{k+1}, based on updated p given by $p^{k+1} = p^k(1 + w\Delta p^k/p^k)$, where w is a weighting factor with $0 < w < 1$.
3) Repeat 1) and 2) until $\Delta p/p$ is less than a preset bound.

III. Problems and Practical Considerations

A. Ambiguity Groups, Testability, and Test Point Selection

In typical circuits, it is common for the column rank of S in (1) to be less than the actual number of circuit parameters; this is due to the presence of ambiguity groups in the circuit [7]. Ambiguity groups are groups of components which cannot be distinguished from each other by measurements made at the designated test nodes and test conditions; consequently, their sensitivity vectors are linearly dependent. Unless the ambiguity groups are eliminated, the sensitivity matrix will be singular, and a solution to (1) cannot be found.

Even with numerically full rank, however, the matrix may still be nearly singular due to near-ambiguity groups. In these cases, the solution is unstable, and will be extremely sensitive to small errors in the model, as well as to small errors in the measurement of Δv. In other words, the testability will be poor [5].

There are several ways in which ambiguity groups, or near-ambiguity groups can be eliminated. The addition of new test nodes or test conditions is often effective. In other cases, it is possible to add additional components of known value between test nodes during testing, making measurements with and without the additional components to increase the rank. Finally, if these approaches are

not feasible or fail, it becomes necessary to reduce the column dimensions of S to rank by artificially fixing the value of all but one component from each ambiguity group at their nominal values. This is accomplished using the QR factorization approach described in [5], [7], and results in a column-reduced sensitivity matrix with full rank. If we represent the column-reduced sensitivity matrix as S_c, then (1) becomes

$$S_c \Delta p_{\text{sel}} = \Delta v \tag{11}$$

where subscript sel represents the selected parameters. Of course, the values of the selected parameters that are members of ambiguity groups can only be estimated relative to the parameters that have been fixed in value.

In this latter approach, the level of ambiguity permitted (and hence, the testability of the selected components) is set by a factor ϵ, provided by the user. By setting ϵ larger, fewer components may be included in S, but the testability of the selected components will be higher. Consequently, response predictions made by substituting the estimated parameter values back into the original model may be more accurate.

After the matrix has been column reduced, then the QR factorization is repeated on the transpose of S_c to reduce the rows to rank, and thereby select a minimum set of measurement times. This square row- and column-reduced matrix, S_{rc}, is used to solve for Δp_{sel}, from measurements Δv_{sel}, made at the selected time points:

$$S_{\text{rc}} \Delta p_{\text{sel}} = \Delta v_{\text{sel}}. \tag{12}$$

Response predictions are made by solving for the predicted deviations, Δv_{pred}, in the following equation:

$$\Delta v_{\text{pred}} = S_c \Delta p_{\text{sel}}. \tag{13}$$

B. Time Skew

In order to obtain accurate parameter estimates from the approach outlined above, it is critical that the timing relationship between the output and input data records be accurately known. In cases where the output and input waveforms are synchronously sampled, this may not be particularly difficult if the external electrical delays are kept equal. On the other hand, it is often convenient to input a standard waveform, e.g., a step, which is known to be nearly ideal, and then sample only the output waveform. In this case, only one recording channel is required, but with asynchronous triggering, the timing may be in error by as much as one half the sampling period. This amount of timing error is often intolerable. For example, it has been found in some cases that as little as 1 ns of time skew can cause changes in parameter estimates on the order of 50 percent. The problem can generally be overcome, however, simply by adding a time skew parameter to the model. We accomplish this by adding an additional component, Δt, to the parameter vector $\Delta p/p$, and an additional column vector, s_{nt}, to the sensitivity matrix, S, where $s_{nt} = dv_n/dt$. The vector s_{nt} is easily computed by taking the first difference of the solution vector from (2), i.e., $s_{nt} = (v_{n+1} - v_n)/h$. It has been verified experimentally that this approach makes the parameter estimates relatively insensitive to the actual time skew.

IV. Example

For an example circuit, a second-order bandpass filter was used, the lumped element model of which is shown in Fig. 1. The step response was simulated based on this model. For greater simulation accuracy, we have used variable size time steps in the numerical integration procedure. For the laboratory tests, a precision programmable step generator developed at NIST was used for the stimulus waveform, and the step response was recorded with a commercial equivalent-time sampling instrument.

The filter was designed to have a nominal center frequency $f_0 = \omega_0/2\pi = 24.5$ kHz, a gain $K = 2$, and a quality factor $Q = 4$. The design values of the elements are given by

$$R_1 = \frac{2Q}{C\omega_0 K} \tag{14.a}$$

$$R_2 = \frac{2Q}{C\omega_0\left\{-1 + \left[(K-1)^2 + 8Q^2\right]^{1/2}\right\}} \tag{14.b}$$

$$R_3 = \frac{1}{C^2\omega_0^2}\left[\frac{1}{R_1} + \frac{1}{R_2}\right] \tag{14.c}$$

$$R_4 = R_5 = 2R_3 \tag{14.d}$$

$$C_1 = C_2 = C = 5 \text{ nF}. \tag{14.e}$$

It is apparent from (14) that, by changing the value of C, other designs are possible that give identical responses. The element values of the actual circuit, however, were within 5 percent of the design values in (14).

The results of an ambiguity analysis of this filter circuit are given in Table I, where the input signal is a step function. It is seen, as expected, that the rank or number of observable components tends to increase as the number of test nodes is increased. Nevertheless, the maximum rank is five (two pairs of ambiguous components remain), even though all test nodes are used. There is no way to distinguish between C_1 or C_2, or between R_1 and R_2, by solely using voltage measurements. However, as shown in the last column of Table I, it is possible to increase the rank to seven (full rank) with as few as one test node, by making additional measurements with known components added to the circuit. In this case, two resistors, R_a and R_b, having nominal values of 1 and 4 kΩ, respectively, were added in succession. R_a was added in parallel with C_1 between nodes 2 and common and R_b was added in parallel with R_5 between nodes 4 and 5. New, perturbed sensitivity matrices, S_a and S_b, are calculated by computing the sensitivity of the new circuits with respect to the seven original components. A composite sensitivity matrix, S_{oab}, is then formed by combining the original and perturbed matrices so that $S_{oab} = [S^T S_a^T S_b^T]^T$. Testability analysis and test point selection can then be performed on S_{oab}. In

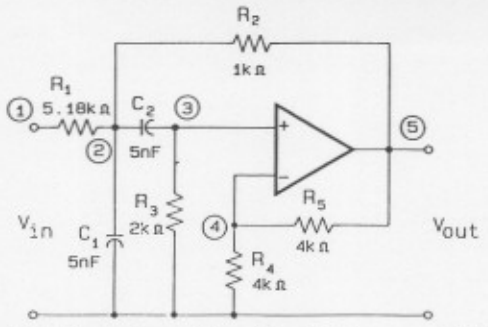

Fig. 1. Model for bandpass filter with center frequency of 24.5 kHz.

TABLE I
TEST NODES AND AMBIGUITY GROUPS

No. of Test Nodes	Test Nodes	Rank	Selected Elements	Rank Using R_a and R_b
1	5	3	R_3, R_2, $[R_1, C_1]^*$	7
	3	3	R_3, R_2, $[R_1, C_1]^*$	7
	2	4	R_3, R_2, $[R_1, C_1]^*[R_4, R_5]^*$	6**
2	3,5	4	R_3, R_2, C_1, $[R_4, R_5]^*$	7
	2,5	5	R_3, R_2, R_1, $[C_1, C_2]^*$ $[R_4, R_5]^*$	7
3	2,3,5	5	R_3, R_2, R_1, $[C_1, C_2]^*$ $[R_4, R_5]^*$	7
4	2,3,4,5	5	R_3, R_2, R_1, $[C_1, C_2]^*$ $[R_4, R_5]^*$	7

* one of two selected depending on the initial values assumed
** all components but R_5

this case, the testability analysis showed the circuit testability to be significantly higher when using two rather than one test node, while increasing the number of nodes to four gave only marginally better testability. Results are presented below using the original sensitivity matrix, S, and then the composite matrix, S_{oab}.

As can be seen in Table I, only three components must be identified in order to predict the complete output (node 5) response. Fig. 2 presents the results of a linear prediction of the step response, based on actual voltage measurements made at node 5, at three time points selected by QR factorization. In this figure, the solid curve is the measured step response, and the dashed curve (barely distinguishable because of coincidence with the solid curve) is the response predicted by solving (13). In this case, the design values, P_d, were used for the calculation of the sensitivity matrix, and the linear model was quite satisfactory.

To determine the effectiveness of the proposed approach for cases in which the nominal values deviate substantially from the actual values, we recomputed the sensitivity matrix based on the assumed values shown in Table II. In this case, the assumed values deviate from the actual values by as much as 100 percent, and result in the large step response differences shown in Fig. 3. Because of the large differences, the linear model is inadequate, as indicated by the poor prediction results shown in Fig. 4. By applying the iterative procedure discussed previously, however, excellent predictions can still be made. Fig. 5 illustrates this, with the prediction results

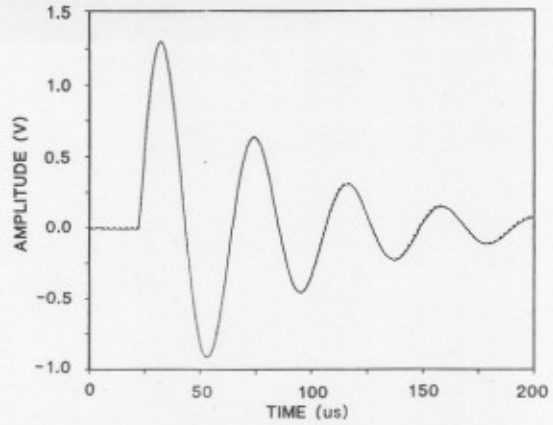

Fig. 2. Measured (solid) and predicted (dashed) step response of filter. The predicted response was based on measurements at three time points, using a single iteration with the sensitivity matrix computed from the design values, P_d.

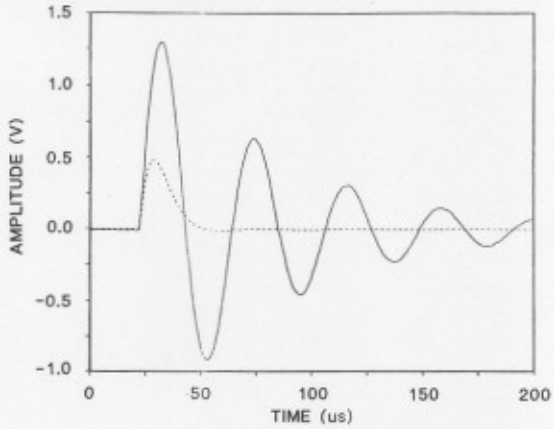

Fig. 3. Measured (solid) and computed (dashed) step response of filter. Computed response was obtained from (6.a) and (6.b), where G and C were calculated using the assumed values, P_0, from Table II.

TABLE II
PARAMETER VALUES (KILOHMS, NANOFARADS)

Component	P_d Design Value	P_0 Assumed Value	$(P_d-P_0)/P_0$ Percent Value	P_u Updated Value
R_1	5.18	5.5	-6	4.815
C_1	5.0	5.2	-4	5.2
C_2	5.0	5.2	-4	5.2
R_2	1.0	1.5	-33	0.967
R_3	2.0	1.0	100	1.993
R_4	4.0	4.0	0	4.0
R_5	4.0	4.0	0	4.0

obtained after four iterations. In this example, a weighting factor, w, of 0.5 was used.

For linear circuits it is sufficient to know the step response, for example, to predict the response to any other input signal. However, for nonlinear circuits, this is not generally the case, and it becomes necessary to determine the full model parameters in order to make accurate response predictions for arbitrary input signals. Therefore, we are interested in the accuracy of parameter estimation and the response predictions made from the original system equations, updated with the new parameter estimates.

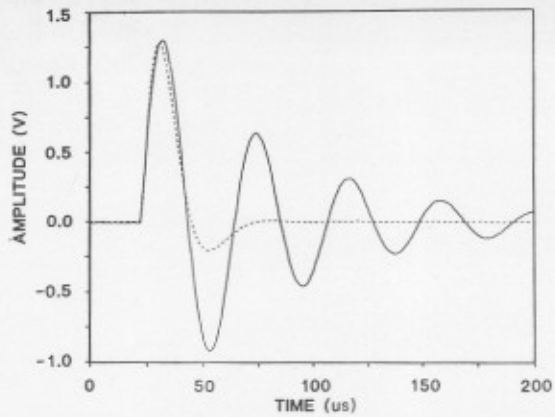

Fig. 4. Measured (solid) and predicted (dashed) step response of filter. Predicted response based on a single iteration, with the sensitivity matrix computed from the assumed values, P_0.

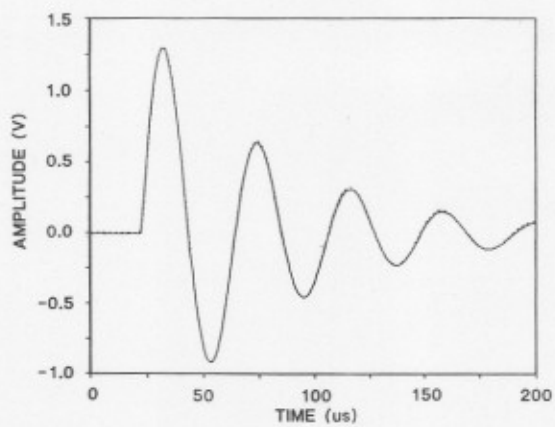

Fig. 5. Same as Fig. 4, after four iterations, using updated values P_u.

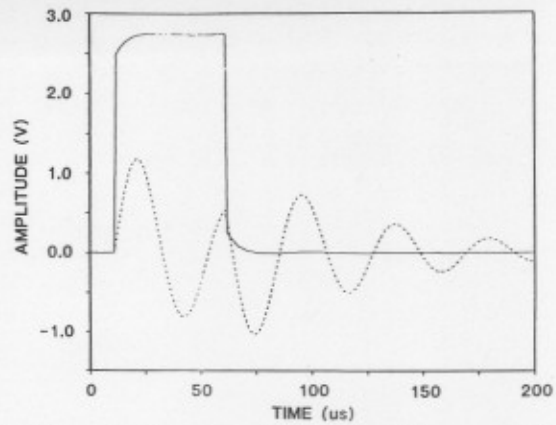

Fig. 6. Measured arbitrary input signal (solid) and the measured filter response (dashed).

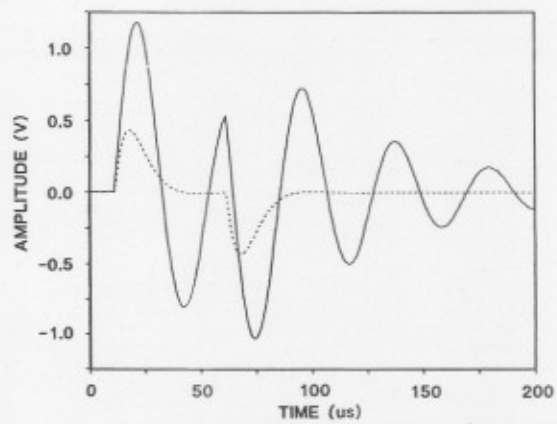

Fig. 7. Measured filter response (solid) and the response computed from (6.a) and (6.b) using the assumed model (dashed), for the arbitrary input signal.

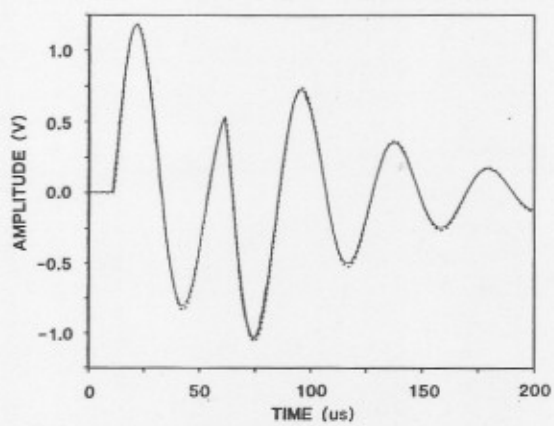

Fig. 8. Measured (solid) and predicted response (dashed) to the input signal of Fig. 6. The predicted response is based on the updated parameter estimates, P_u, determined from step response data.

The results from such a prediction are given in Figs. 6 and 7. Fig. 6 shows an arbitrary input signal (solid) and the measured filter response (dashed). In Fig. 7 we show the measured filter response (solid) and the response predicted from the assumed model (dashed), which is based on assumed values P_0. Finally, Fig. 8 shows the predicted response to the input signal of Fig. 6, computed from the updated parameter estimates, P_u, determined earlier from step response data. The peak error in the prediction is less than 2 percent.

The updated parameter values that were used for the predicted response in Fig. 8 are given in Table II. These are also the values that were used to obtain the response prediction of Fig. 5. Note that the updated values of the selected elements, R_1, R_2, and R_3, deviate significantly from the design values. This is because these elements form ambiguity groups with unselected components whose values have been arbitrarily fixed at the assumed values listed in Table II. Any error in the value of an unselected component will be compensated by the computed deviation for the selected component. Thus for example, the filter response depends on $\alpha = 2Q/\omega_0 K = R_1 C$, rather than on R_1 and C independently. For small deviations, the net effect of time constant $R_1 C_1$ will be constant, independent of the exact choice of C_1. In these cases, as indicated in Fig. 8, the predicted responses will be accurate even though the individual parameter estimates are not.

Results are given in Table III for the case in which additional measurements were made on the circuit perturbed by the addition of components R_a and R_b, as described

TABLE III
PARAMETER VALUES USING R_u AND R_b (KILOHMS, NANOFARADS)

Component	P_d Design Value	P_0 Assumed Value	$(P_d-P_0)/P_0$ Percent Change	P_u Updated Value	$(P_d-P_u)/P_u$ Percent Change
R_1	5.18	5.0	3.6	5.136	0.86
C_1	5.0	5.2	-3.9	5.044	-0.87
C_2	5.0	5.25	-4.8	5.089	-2.15
R_2	1.0	1.2	-17	1.008	-0.79
R_3	2.0	1.8	11	2.039	-1.91
R_4	4.0	3.5	14	4.033	-0.82
R_5	4.0	3.4	18	4.029	-0.72

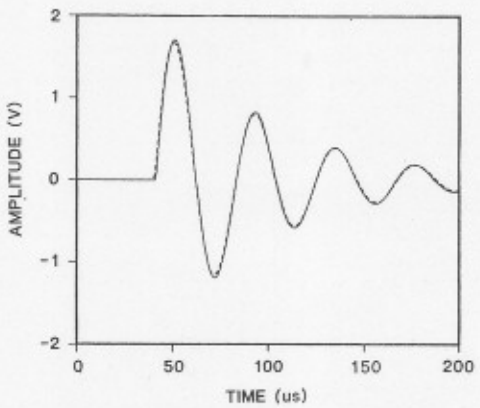

Fig. 9. Measured step response (solid), and step response predicted (dashed) from measurements made on the original and perturbed circuits.

earlier. In this case, measurements were made at test nodes 2 and 5, on both the original and perturbed circuits. As seen in the fourth column, the assumed values (P_0) of the components deviated by as much as 18 percent from the design values. After eight iterations, the updated estimates (P_u) listed in column five were obtained. The updated values deviate from the design values by only about 2 percent, which is within the design tolerances. In Fig. 9, the step response predicted using the updated values is plotted. The solid curve is the measured step response, and the dashed curve is the step response calculated using (6.a) and (6.b), where matrices G and C have been recomputed based on the updated values.

V. CONCLUSION

An efficient approach for parameter estimation and time-domain response prediction of analog circuits has been presented. The test equations, which can be generalized to include nonlinear circuits, are based on the sensitivity matrix which can be obtained simultaneously with the nominal solution vector. An iterative parameter estimation approach is used when the element values deviate substantially from the nominal design values.

The effects of ambiguity groups were shown to be very important for parameter estimation, and techniques for reducing their number or algebraically accomodating them, were presented. In particular, it was shown that additional measurements made on a circuit perturbed by the insertion of components of known value between critical test nodes can break ambiguity groups. This approach could form an attractive compromise between functional testing and traditional bed-of-nails, in-circuit testing.

Directions for future work include improvements in the numerical integration and optimization routines, and extensions to accomodate mixed-signal devices and nonlinear elements. With regard to nonlinear networks, methods for selecting suitable test waveforms will also require further study.

ACKNOWLEDGMENT

The authors have benefited in this work from valuable discussions with J. Starzyk of Ohio University and G. Stenbakken of NIST. In addition, valuable assistance was received from D. Flach and P. Hetrick of NIST, who performed the measurements on the test circuits.

REFERENCES

[1] E. Flecha and R. DeCarlo, "Time domain tableau approach to the fault diagnosis of analog nonlinear circuits," in *Proc. IEEE Int. Symp. Circuits and Systems*, Newport Beach, CA, pp. 828–830, 1984.

[2] R. Saeks, A. Sangiovanni-Vincentelli, and V. Visvanathan, "Diagnosability of nonlinear circuits and systems—Part II," *IEEE Trans. Circuits Syst.*, vol. CAS-28, pp. 1103–1108, 1981.

[3] V. Visvanathan and A. Sangiovanni-Vincentelli, "A computational approach for the diagnosability of dynamical circuits," *IEEE Trans. Computer-Aided Design*, vol. CAD-3, pp. 165–171, 1984.

[4] G. N. Stenbakken *et al.*, "Efficient calibration strategies for linear, time invariant systems," in *Proc. 1985 AUTOTESTCON*, Long Island, NY, pp. 361–366, Oct. 1985.

[5] G. N. Stenbakken and T. M. Souders, "Test point selection and testability measures via QR factorization of linear models," *IEEE Trans. Instrum. Meas.*, vol. IM-36, pp. 406–410, June 1987.

[6] J. Vlach and K. Singhal, *Computer Methods for Circuit Analysis and Design*. New York: Van Nostrand Reinhold, 1983.

[7] G. N. Stenbakken, T. M. Souders, and G. W. Stewart, "Ambiguity groups and testability," *IEEE Trans. Instrum. Meas.*, vol. 38, pp. 941–947, Oct. 1989.

STEP AND FREQUENCY RESPONSE TESTING OF WAVEFORM RECORDERS

T. M. Souders, D. R. Flach
National Institute of Standards and Technology

and

J. J. Blair
EG&G Energy Measurements

Abstract

Tutorial material is presented to aid in measuring the step response of waveform recorders, and to compute other parameters which may be derived from it. Parameters considered include impulse response, transition duration, settling time, and complex frequency response. The measurement approaches follow those recommended in the IEEE "Trial Use Standard for Digitizing Waveform Recorders." Illustrated examples are given, and guidelines on the choice of step generators are also included.

I. INTRODUCTION

Some of the most revealing measures of a waveform recorder's dynamic performance can be computed from its step response. These not only include such time-domain parameters as impulse response, transition duration (rise time), settling time and overshoot, but also frequency domain parameters such as bandwidth, frequency response (both amplitude and phase), and gain error.

Many of these performance parameters are defined in the recently published IEEE Standard 1057, "Trial Use Standard for Waveform Recorders," [1], and suitable test methods for measuring the parameters are recommended in the same document. In this paper, supplementary information is given to help the user correctly implement those tests that are based on step response, and practical illustrated examples are included. Some guidelines on the choice of step generators are also included.

In one case, a suggested method is outlined which differs from a corresponding one included in the IEEE Standard. This method, a technique for extracting equivalent-time sampling information, was developed subsequent to the adoption of the Standard, and is considered by the authors (of this paper) to be better and easier to implement than the one outlined in that document.

The use of step response measurements to obtain frequency response information continues to cause some confusion for those not familiar with the technology. This situation is reinforced by the prevalent use of sine wave tests elsewhere in the Standard to obtain information such as nonlinearities. This seemingly inverted state of affairs arises from the nature of waveform recorders and the economics of the measurements. First of all, waveform recorders are inherently time-domain instruments: time is always the independent variable. Second, sine waves are chosen for linearity measurements as much because they are easily generated and their purity is relatively easy to control, as they are because of their singular importance in the frequency domain. Third, obtaining frequency responses with step signals is orders of magnitude easier than obtaining them with sine waves.

II. EQUIVALENT-TIME TESTING

A common limitation that is encountered when computing step and frequency response parameters from sampled step response data is the relatively small ratio of sampling rate to bandwidth which is characteristic of typical waveform recorders. Typical values (ranging from two to four) produce coarse time quantization in the time domain, and give rise to substantial aliasing errors in the frequency domain if the input signal is not band-limited. It would therefore be desirable to effectively increase the sampling rate of the waveform recorder when making these measurements. Such an approach is suggested in Standard 1057; a similar method, considered better by the authors, is outlined next.

The Concept

If the input signal is repetitive, the sampling rate limitations can be reduced by using the principle of equivalent time sampling to multiply the effective sampling rate of the waveform recorder by an integer, D. This is illustrated in fig. 1 for D=4. By choosing the repetition rate of the input step appropriately, D=4 periods are recorded in a single record (bottom); then, upon rearranging the samples (top) with a simple algorithm, a single repetition is obtained which is effectively sampled at D times the original sampling rate. In this example, the hypothetical waveform recorder has a single pole transfer function and a ratio of sampling rate to bandwidth of 3.14 (π). Note that the rising edge is sampled very coarsely. If the frequency response were computed directly from this data, the aliasing errors would be quite large. Using

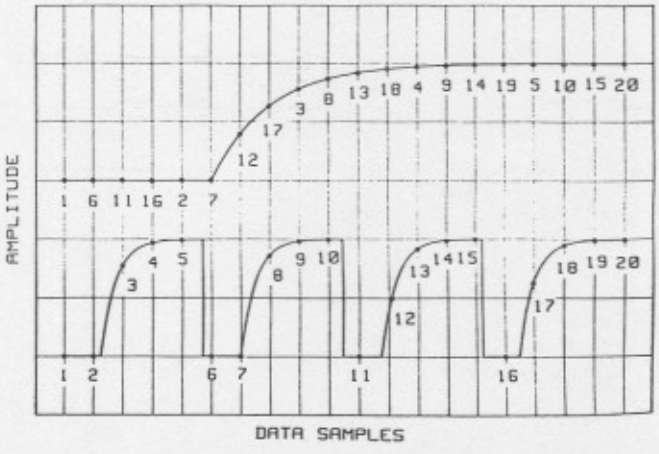

Fig. 1 Illustration of equivalent-time sampling approach. The bottom waveform shows the real-time samples and the top waveform has been reconstructed in equivalent-time from the bottom waveform by rearranging the samples as indicated.

CH2735-9/90/0000-0214$1.00 C 1990 IEEE

the bounds for aliasing errors given in section 4.7.2 of [1], the estimation of bandwidth from such a determination could be in error by as much as 40%. However, using the reconstructed step response at the top, the errors would be reduced to 2.5%.

The following BASIC program implements the algorithm to rearrange the samples in equivalent time:

```
10   C=0
20   FOR I = 1 TO L
30   FOR J = 1 TO D
40   C = C + 1
50   I2 = I + (J-1)*L
60   E(C) = R(I2)
70   NEXT J
80   NEXT I
```

Where D — (integer) sampling rate multiplier
M — record length
L — INT(M/D) and INT(*) designates the integer part of *
E(*) — array containing equivalent-time samples
C — equivalent-time sampling index
R(*) — array containing real-time samples
I2 — real-time sampling index

The numbers adjacent to the equivalent-time samples in the top plot of fig. 1 indicate the corresponding sequence of real-time samples from the bottom plot.

Selection of Parameters

The selection of parameters required is straight forward. First, integer D is chosen based on the required equivalent sampling rate, f_{eq}, such that $f_{eq} = Df_s$, where f_s is the (real-time) sampling rate of the waveform recorder. Next, L, the number of real-time samples taken during each repetition of the step, is given by INT(M/D), i.e., the integer value of M/D, where M is the number of samples in a record. Finally, the step generator's repetition rate, f_r, is eet such that

$$f_r = f_s \left(\frac{D}{L \times D - 1} \right), \quad L \times D \leq M \tag{1}$$

For the example of fig. 1, D = 4, L = 5, and $f_r = 0.2105263\ f_s$. Note that data points between M and D*INT(M/D) are not usable. (Since this equivalent-time test method differs from that in Standard 1057, Eq. 1 differs from the corresponding equation in section 4.1.5.1 of that standard.)

Accuracy Requirements

This method of achieving higher equivalent sampling rates requires that the repetition rate, f_r, of the step generator be precisely controlled. While the average equivalent-time sampling rate is just $D \times f_s$, independent of f_r, the relative spacing of the equivalent-time samples becomes non-uniform when f_r deviates from the value given by Eq. 1. If f_r is too great, D-1 out of D successive samples will occur too late while one sample will be correctly placed; if f_r is too small, D-1 samples will occur too soon. In either case, the maximum sampling time error is given, to a good approximation, by

$$\frac{\Delta t_{eq}}{t_{eq}} \approx M(D-1) \frac{\Delta t_r}{t_r} \tag{2}$$

where t_{eq} — the average equivalent-time sampling period, i.e., $1/Df_s$
Δt_{eq} — the maximum sampling time offset
$\Delta t_r/t_r$ — proportional error in the repetition period (or repetition rate)

Note, however, that the errors are not cumulative; the average equivalent sampling period is still given by $1/Df_s$.

Of course, the assumption is made in Eq. 2 that f_s is exactly known; if it is not, then additional error given by an expression similar to Eq. 2, will accrue. As an example, if D is four, the record length is 1024, and the equivalent sampling period is to be known to 5%, then the repetition rate must be set, and the sampling rate must be known, each with an accuracy of 0.05/(1024*3) = 16 ppm. To achieve such accuracies, it is usually necessary to trigger the step generator with an external, frequency synthesized source. It may sometimes be necessary to measure the frequency of the step as well as the waveform recorder's clock frequency with an accurate frequency counter to assure that they are set with sufficient accuracy.

Tradeoff Between Accuracy and Spectral Resolution

If sufficient accuracy cannot be achieved for a given record length, the accuracy can be improved directly by decreasing the length of record used. However, since the lowest frequency component that is represented in a record of length M is given by f_{eq}/M, this limits the range of frequencies that can be represented when the frequency response is computed.

III. COMPUTATION OF FREQUENCY RESPONSE

As recommended in Standard 1057, two basic steps are required in the computation of frequency response from the step response data. First, the step response data is numerically differentiated to obtain the discrete impulse response. This is performed with the following equations:

$$I_n = (S_{n+1} - S_n) / t_{eq}, \quad 1 \leq n < M \tag{3a}$$

$$I_n = (I_{n-1}) / t_{eq}, \quad n = M \tag{3b}$$

where I_n — nth impulse response sample
S_n — nth step response sample
t_{eq} — the equivalent-time sampling period

Next, the Fourier transform of the discrete impulse response is taken to obtain the frequency response. If the impulse response does not begin very near the start of the record, it is first advisable to delete a portion of the record so that the impulse does begin near the start; otherwise, a large linear phase term will result in the subsequent phase plot.

Example

Figs. 2-9 illustrate, with laboratory results taken on a commercial waveform recorder, the entire sequence of operations required to obtain the complex frequency response: obtaining step response data, rearranging the data to obtain equivalent-time samples, computing the impulse response, computing the frequency response, and plotting the magnitude and phase spectra in different formats.

In fig. 2, the raw step response data from the waveform recorder is plotted. In this example, D=4, M=4095, L=1023, f_s=60 MHz, and f_r=58.66536 kHz. The input step is approximately ± 0.9 V, from a fast-settling

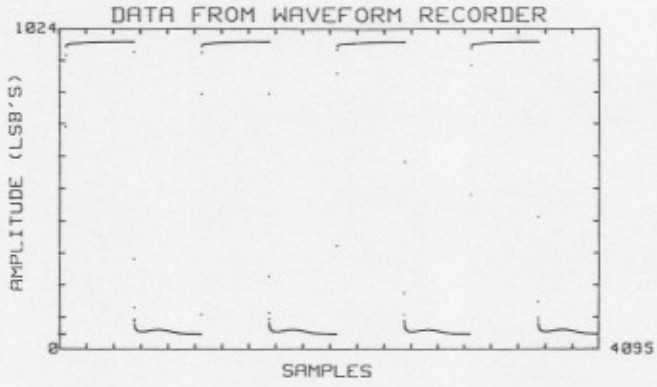

Fig. 2 Data from a 10-bit waveform recorder with a repetitive input step. The repetition rate has been chosen to give an equivalent sampling rate of four times the actual rate, after rearranging the samples.

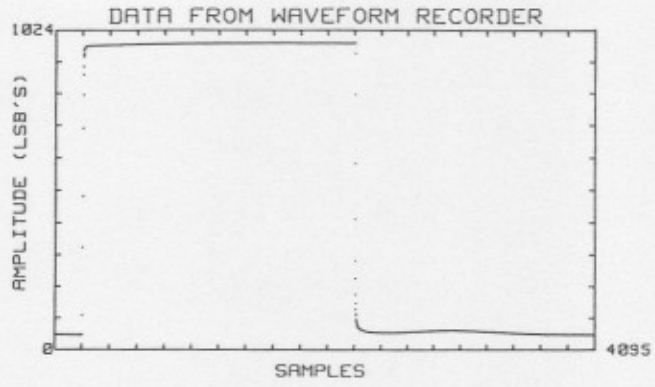

Fig. 3 The data from fig. 2 after rearranging the samples as specified in the text.

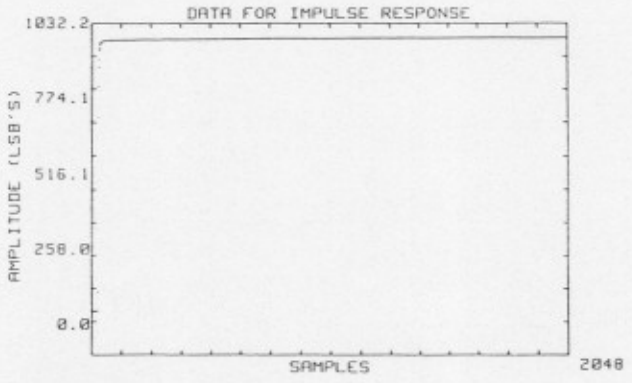

Fig. 4 The portion of data from fig. 3 selected for the impulse response computation.

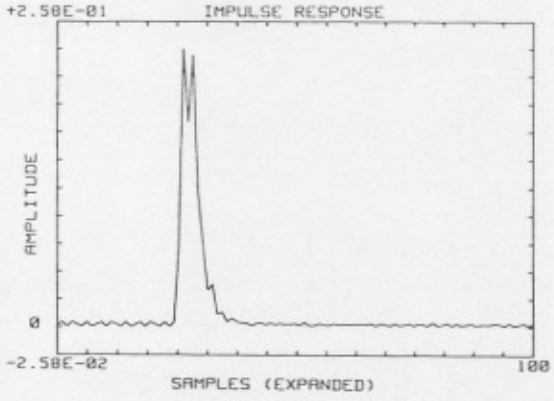

Fig. 5 A time expanded plot of the discrete impulse response computed from the data plotted in fig. 4.

generator developed at NIST [2]. (The generator is designed to give the rated performance for only a selected transition polarity; in this case the positive transition was selected, and only data from that transition is subsequently used.)

The data plotted in fig. 3 has been rearranged using the algorithm given previously; note the increase in the effective sampling rate. In fig. 4 is plotted a subset of the data that has been selected for subsequent processing. Much of the initial, pre-step waveform has been deleted as well as the negative transition. (Deletion of the negative transition is mandatory, because only a single step must be used.)

A time-expanded plot of the impulse response, computed from Eq. 3, is given in fig. 5. The occurrence of substantial noise on the computed impulse response is typical because differentiation accentuates noise. However, the spectral components of the noise are typically quite high and cause little problem in the frequency range of most interest, i.e., below the cutoff frequency. If the noise must be reduced, the digital filter described in [1] and [3] is quite effective.

Fig. 6 gives the resulting magnitude spectrum obtained by performing an FFT on the impulse response data. The spectral lines have been normalized to the amplitude of the first (non-dc) line. The waveform recorder's gain flatness versus frequency is more readily apparent in fig. 7, where the deviations from the first spectral line are plotted on a split log-log scale.

The raw phase information obtained from the FFT of the impulse response is plotted in fig. 8. As with most FFT routines, the phase information is presented modulo π, i.e., only the remainder after dividing by π is given. To obtain the true, cumulative phase plot, a short program is written to add 180° following each 180° discontinuity. Noise will usually impose a limit on how high in frequency such an approach can be effective. Eventually, when the frequency components are sufficiently small, the noise will cause additional discontinuities large enough to fool the unraveling algorithm. In addition to the unraveling process, the residual linear-phase term, caused by an arbitrary time shift of the impulse response with respect to the start of the record, should be removed to accentuate the nonlinear phase response. This is accomplished by rotating the phase plot about its origin, so that it passes through some nominal, expected value at a given

frequency. As an example, most waveform recorders exhibit a dominant pole which determines the bandwidth or cutoff frequency; at this frequency, the phase angle should nominally be -45°. Therefore, it is sometimes convenient to rotate the phase plot so that it passes through -45° at the cutoff frequency. Fig. 9 shows the results of unraveling and removing the linear phase term from the raw phase data of fig. 8.

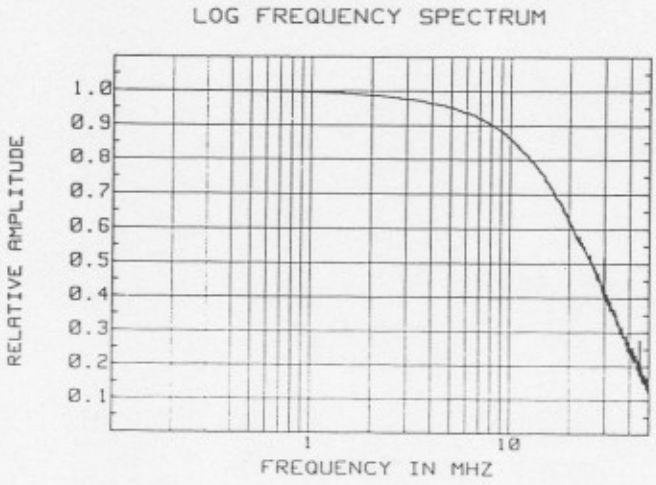

Fig. 6 The magnitude spectrum of the waveform recorder, computed by taking the FFT of the discrete impulse response, a portion of which is shown in fig. 5.

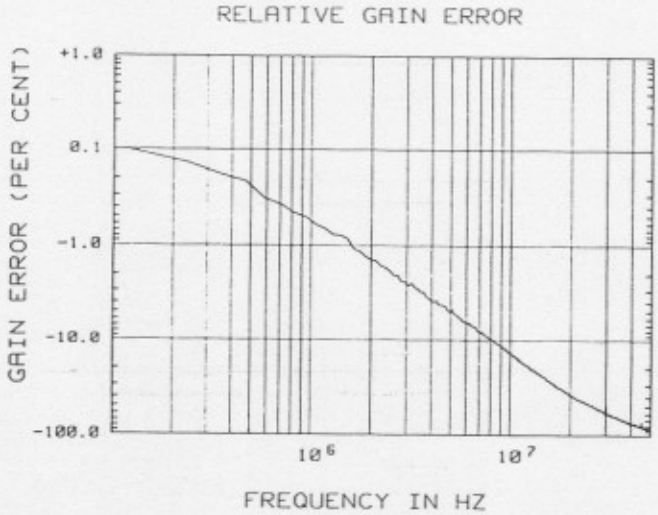

Fig. 7 The gain flatness computed as the deviation of the magnitude spectrum from the first spectral line.

IV. SETTLING PERFORMANCE

The following four figures illustrate the measurement of settling time, short-term settling time, and long term settling error using the definitions and procedures as recommended in Standard 1057. The figures represent the settling performance of a 10-bit waveform recorder with an input step whose baseline and topline were 5 and 95 percent of full-scale, respectively, giving a step amplitude of 90% of full-scale. Two records were taken of 4095 points each, at respective sampling rates of 30 and 1 MHz, giving

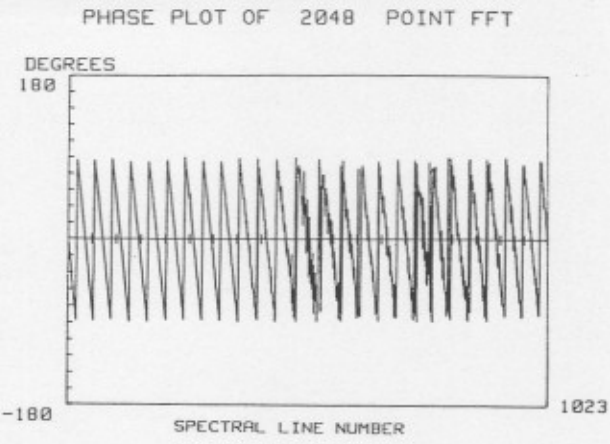

Fig. 8 Raw phase data (modulo π) from the FFT of the impulse response.

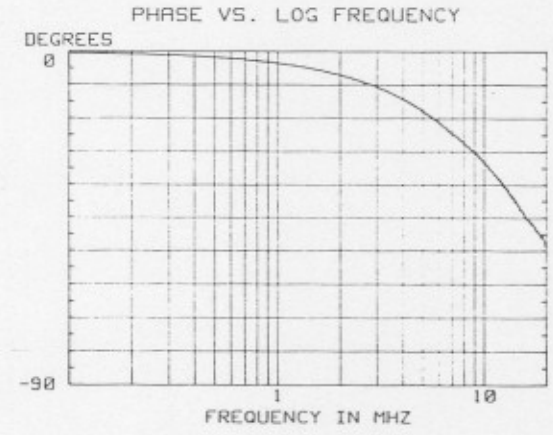

Fig. 9 Phase spectrum after unraveling raw phase data and removing the unwanted linear phase component.

respective time epochs of 0.1365 and 4.095 ms. It can be seen that the recorder exhibits both short and long term settling responses, appearing to have settled within the time epoch of fig. 10, but showing subsequent longer term settling behavior over the longer epoch represented in fig. 11. In other records extending out to 1 s, no significant additional settling was observed. In fig. 10, the horizontal dashed lines represent an error band of ± 0.56% of the input step amplitude (5 LSB's) about the final value of the record, and the vertical dashed line represents the point at which the waveform last enters the error band. The short-term settling time is the duration from the proximal point of the transition (occurring at the 256th sample) to the time represented by the vertical dashed line; this duration is (422-256) sample periods or 5.53 μs in this example. The long-term settling error is the difference between the final value measured at 1 s (represented by the solid horizontal line), and the final value in this record. In this example, the long-term settling error is 7 LSB's or 0.78% of the input step amplitude.

In fig. 11, the final value essentially coincides with the value at 1 s, and the horizontal dashed lines thus designate the error band for settling time as opposed to short-term settling time.

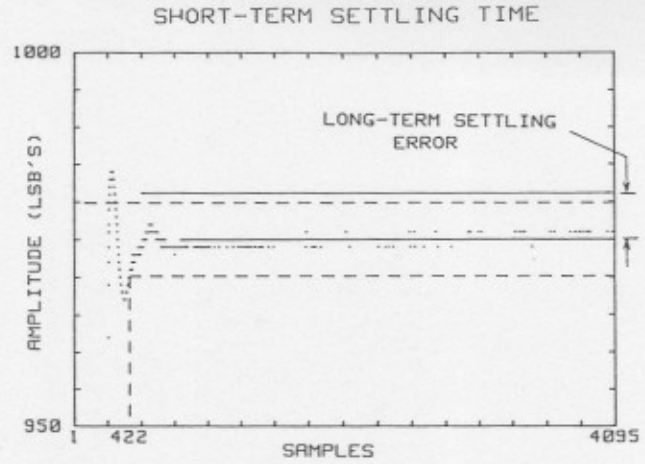

Fig. 10 Short-term settling performance of a 10-bit, 30 MHz recorder. The input step begins at the first sample division (256th sample). The short-term settling to 5 LSB's is shown with the dashed lines to occur at the 422nd sample, giving a short-term settling time of 5.5 μs. The long-term settling error is shown as the deviation of the final value in the record from the final, dc value of the step response (solid horizontal line).

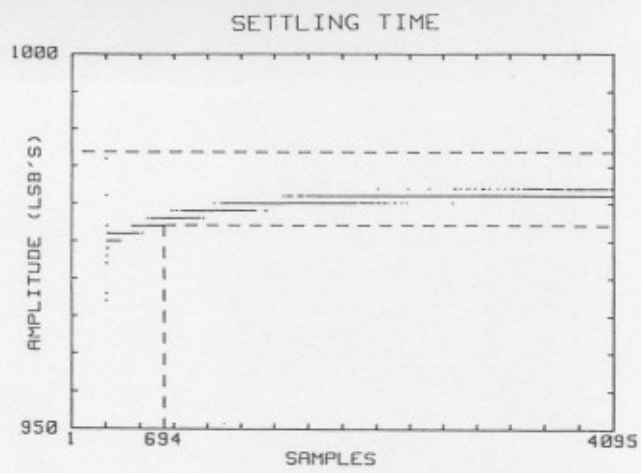

Fig. 11 The settling performance of same recorder as in fig. 10 over a longer time epoch. The sampling rate is 1 MHz in this example, and the settling time is (694-256)×1 μs = 438 μs.

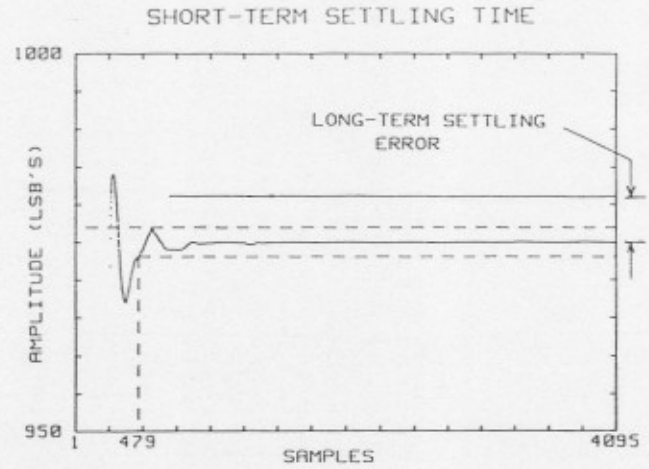

Fig. 12 The settling performance determined by prefiltering the data of fig. 10 to reduce noise and quantization errors. The error band shown is ± 2 LSB.

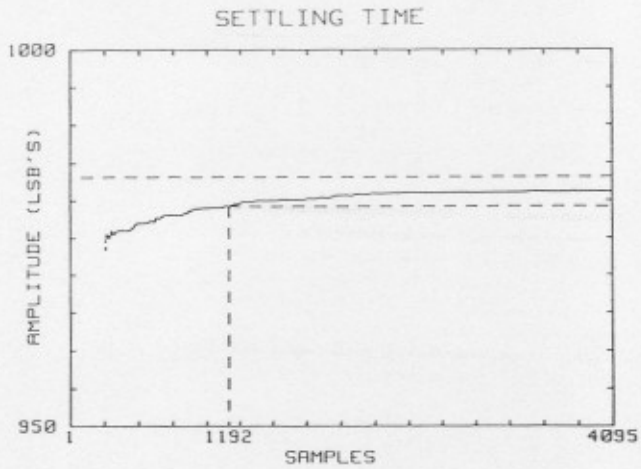

Fig. 13 The settling performance determined by prefiltering the data of fig. 11 to reduce noise and quantization errors. The error band shown is ± 2 LSB.

Note that noise and quantization errors limit the measurement of settling performance. To some extent, these limitations can be overcome by digitally pre-filtering the data before determining the settling performance. Examples in which a moving average filter has been used are given in figs. 12 and 13. These correspond to those of figs. 10 and 11, but with tighter error bounds (± 2 LSB's). Note that the use of filtering in settling time measurements is NOT addressed in the Standard, and that improper use of filtering can dramatically alter the apparent settling performance, as well as minimize noise and quantization errors.

V. CHOOSING A STEP GENERATOR, AND ANALYSIS OF ERRORS

A number of criteria should be kept in mind when selecting a step generator to perform the measurements discussed above. These include the generator's transition duration, settling performance, time jitter, and programmability, as well as its output impedance and means for connection to the recorder under test. These are each addressed in the following sections.

Transition Duration

As a rule-of-thumb, the transition duration of two linear systems in cascade is the root-sum-of-squares of the individual transition durations. This rule is exact if the step response is monotonic and the

transition duration is defined as the 10-90 percent transition duration of a Gaussian system with the same dispersion [4]. If transition duration is defined conventionally as in IEEE Standard 194 on pulse terms and definitions [5], then the rule is only an approximation; nevertheless, for many systems of interest, it gives reasonable results.

According to Standard 1057, the step generator should have a transition duration no greater that one fourth that expected of the waveform recorder under test. Using the-rule-of-thumb, this bound represents an error contribution to the measurement of transition duration T, of approximately $\{[T^2+(T/4)^2]^{1/2} - T\}/T = 3\%$. The same rule-of-thumb can be used to estimate the error which results if a slower step generator is used.

Settling Time

The settling time definition of Standard 1057 uses two parameters, an error band, ϵ, and a settling time, t. By that definition, a waveform recorder satisfies the settling time conditions $[\epsilon,t]$ if its step response remains within $\pm\ \epsilon$ of its final value for all time later than t. The settling performance of the input step of course affects the measured settling time of the waveform recorder. As a rule-of-thumb, if $[\epsilon,t]$ is the settling time requirement to be demonstrated from the waveform recorder, then the input step used for testing should simultaneously satisfy the two settling time requirements, $[\epsilon,t/k]$ and $[\epsilon/k,t]$, to achieve an accuracy of 1/k in the determination of t. In the IEEE Standard, it is recommended that k be four or greater. This rule is demonstrably sufficient for one and two pole systems; it should also provide a resonable bound for other, more complex responses.

Time Jitter and Timing Accuracy

The time-domain effects of errors in setting the repetition rate were outlined in a previous section on equivalent-time testing. In the frequency domain, the resulting nonuniform sampling causes errors in the computed frequency response. While a general formulation of the spectra of nonuniformly sampled signals has been derived in [6], the examples given in that paper have only been worked out for sinusoidal inputs. We can put the problem into perspective by considering the case in which the input is an ideal step, the sample time errors are small, and the waveform recorder has an ideal, single pole response with cutoff frequency f_{co}. Fig. 14 gives the errors in the magnitude spectrum resulting from sampling time errors for the following sampling conditions: the sampling rate multiplier (D) is 5, the record length (M) is 4096, the error in repetition rate (f_r) is 25 ppm, and the ratio of sampling rate to bandwidth (f_s/f_{co}) is 2.5. The plot in this figure can serve as a guideline for estimating frequency response errors due to errors in setting the repetition rate, f_r. For errors in the sampling times ($\Delta t_{eq}/t_{eq}$) that are less than 100% (see Eq. 2), the errors in frequency response scale directly with sampling time errors; likewise, the errors scale directly with record length, M. As the ratio f_s/f_{co} increases, the spectral error peaks shift to higher frequencies with respect to f_{co} without changing appreciably in magnitude. Changes in D (over the range of 2 to 12) cause the peak error to change by $\pm$ 50% from the value at D=5.

Timing jitter causes randomly distributed displacement of the sampling times, which in turn causes equivalent amplitude noise in the sampled step response signal proportional (to first order) to the derivative of the step response. In the frequency domain, after differentiating and taking the Fourier transform, the net effect is a noise spectrum with most of the energy concentrated above the cutoff frequency.

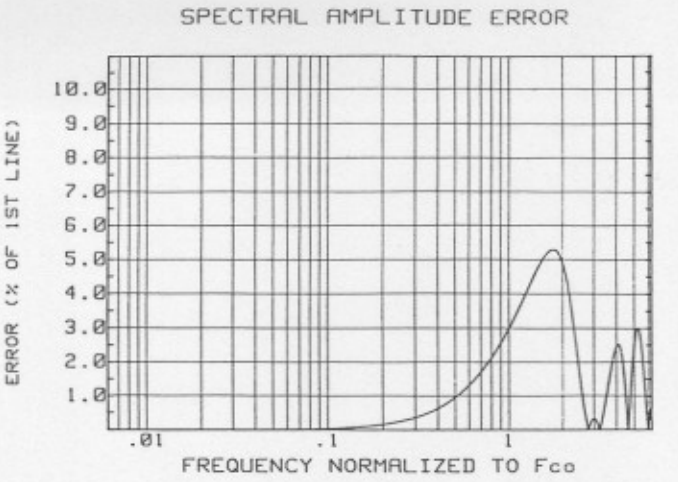

Fig. 14 Plot of the spectral magnitude errors, resulting from a 25 ppm error in setting step repetition rate. In this example, the ratio of f_s to f_{co} is 2.5, D=5, and M=4096.

Programmability

The previous sections make it clear that the step generator's repetition rate must be setable to odd values with high accuracies in order to insure accurate equivalent-time timing accuracy. It is also desirable to have the amplitude and step polarity be variable as well. This is useful in matching the step amplitude to multiple input ranges of the recorder under test, and to check the assumption of linearity that is made when computing frequency response from step response data. As an alternative, different amplitudes can be obtained with external, high quality attenuators. In either case, it is instructive to record the step response at two or more amplitudes, and compare the frequency responses computed from each. If the recorder is linear, then the two plots will be identical, within the noise limits of the process. If the recorder is nonlinear, then the plots will diverge at some frequency.

Transmission Line Considerations

For best results, the step generator should be terminated through a matched cable in its characteristic impedance, preferably with the input impedance of the recorder itself, and the generator should be connected to the recorder through the shortest length of cable practicable. Taking these steps will minimize distortion of the step due to reflections and dispersion.

The important thing to remember when considering the losses due to cables is that the transition and settling times for skin effect limited coaxial cables are proportional to the square of the length of cable [6,7]. When passing a unit step through a skin effect limited coaxial cable the output is 1-e(t), where the error, e(t), is given by

$$e(t) \simeq C\ \ell\ t^{-1/2} \qquad (4)$$

where ℓ is the length in feet, t is the time in nanoseconds and C is a constant depending on the particular type of cable. This formula is valid for t large enough that $e(t) \leq 0.5$, and is derived by

approximating the step response formula given in [7]. The value of C for RG-58 cable is 0.0058. Table I gives the errors computed from Eq. 4 for several times and three lengths of cable . Note that the error dies out very slowly and therefore is quite serious in measurements of settling performance.

Table I

RESPONSE ERROR DUE TO CABLE LOSS (RG-58)			
Time (ns)	Error (%)		
	1/10 ft	1 ft	10 ft
1	0.058	0.58	5.8
2	0.041	0.41	4.1
5	0.026	0.26	2.6
10	0.018	0.18	1.8
20	0.013	0.13	1.3
50	0.008	0.08	0.8
100	0.006	0.06	0.6

VI. CONCLUSION

The measurement approaches and suggestions given in this paper are intended to be used in conjunction with the IEEE Trial Use Standard for Digitizing Waveform Recorders. That document includes definitions, test methods and conditions of test which have been tacitly assumed in this paper. A particularly important point to keep in mind is that aliasing errors will always be present when sampling step response with a finite sampling rate, and formulae for computing bounds on those errors are included in the Standard.

The authors hope that the examples and suggestions presented here will take some of the mystery out of step response testing and deriving time- and frequency-domain information from those tests. Any difficulties in implementing these tests, or suggestions for improvements, should be directed to the authors or the Waveform Measurements and Analysis Committee of the IEEE Instrumentation and Measurement Society which developed the Standard.

REFERENCES

1. IEEE Standard 1057, IEEE Trial-Use Standard for Digitizing Waveform Recorders, July 1989.

2. H. K. Schoenwetter, "Design and Characterization of a Programmable Step Generator with Very Fast Settling Performance," IEEE Trans. Instrum. Meas., vol. IM-36, no. 2, June 1987.

3. T. M. Souders and D. R. Flach, "Accurate Frequency Response Determinations from Discrete Step Response Data," IEEE Trans. Instrum. Meas., Vol. IM-36, no. 2, June 1987.

4. J. J. Blair, "On the Effect of Linear Systems on Transients," IEEE Trans. Instrum. Meas., Vol. IM-22, no. 3, September 1973.

5. IEEE Standard 194-1977, IEEE Standard Pulse Terms and Definitions, 1977.

6. Y. C. Jenq, "Digital Spectra of Nonuniformly Sampled Signals: Fundamentals and High-Speed Waveform Digitizers," IEEE Trans. Instrum. Meas., Vol. IM-37, no. 2, June 1988.

7. R. L. Wiggington and N. S. Nahman, "Transient Analysis of Coaxial Cables Considering Skin Effect," Proc. IRE, Vol. 45, Feb. 1957.